Monthly Notices
of the
ROYAL ASTRONOMICAL SOCIETY

MNRAS **453,** 4485–4499 (2015) doi:10.1093/mnras/stv1709

Absolute polarization determinations of 33 pulsars using the Green Bank Telescope

Megan M. Force,[1] Paul Demorest[2] and Joanna M. Rankin[1]★

[1]*Physics Department, University of Vermont, Burlington, VT 05405, USA*
[2]*National Radio Astronomy Observatory, Socorro, NM 87801, USA*

Accepted 2015 July 27. Received 2015 July 7; in original form 2014 April 14

ABSTRACT

Absolute polarimetry observations of 33 pulsars were carried out with the Green Bank Telescope in the 1100–1900 MHz band using the Green Bank Ultimate Pulsar Processing Instrument. This group was selected to help complete a larger sample for which accurate proper-motion measurements were available. A combination of profile analysis using the core/double cone model and polarization-angle fitting methods were applied to estimate the 'fiducial' longitude of the magnetic axis for each star and refer the linear polarization angle at that point to infinite frequency. As had been found previously, a number of the pulsars are found to have fiducial polarization directions that fall either along or at right angles to their proper-motion directions, whereas upwards of a third of the stars studied show alignments that are neither parallel nor orthogonal.

Key words: pulsars: general.

1 INTRODUCTION

Pulsars have been observed to travel at high space velocities, sometimes exceeding 1000 km s^{-1}. Theorists have suggested various mechanisms by which an asymmetry in the supernova of a pulsar's stellar progenitor might deliver a high-velocity 'kick' to the neutron star remnant (e.g. Spruit & Phinney 1998). In the interest of investigating the origins of the high velocities observed, various groups have undertaken studies of the relative orientation between the directions of linear polarization of pulsars and their proper motions. This work, a study of the absolute polarimetry of 33 pulsars observed with the Green Bank Telescope (hereafter GBT) in West Virginia, adds to the body of knowledge gathered by these groups, and amplifies the conclusion, first clearly articulated by Johnston et al. (2005; hereafter Johnston I) that many pulsars exhibit orderly alignments between their linear polarization and proper-motion (hereafter PM) directions on the sky.

Inspired by the work of Johnston I, a number of further alignments were assembled by Rankin (2007), adding 26 pulsars to Johnston's original sample. A third study by Johnston et al. (2007; hereafter Johnston II) followed shortly thereafter, and a re-evaluation of the existing alignments using 54 pulsars was published by Noutsos, Kramer & Carr (2012).

Investigations into pulsars' large space velocities and the orientations of supernova 'kicks' are, however, much older than Johnston I. In an effort to explore these questions, major surveys of absolute linear polarimetry were pioneered by the Bonn group (Morris et al. 1979, 1981, hereafter MGSBT); these failed to show PM alignments. Factors leading to this failure included the small sample then available, inaccurate timing PMs and central longitudes, and in a few cases poorly determined rotation measures (hereafter RM). Deshpande, Ramachandran & Radhakrishnan (1999) encountered a similar difficulty as late as 1999.

Following the widespread presumption that pulsars emit by the curvature process, it seemed that the orientation of the linearly polarized radiation must be parallel to the projected magnetic field direction. Even after the discovery that pulsars emit in two orthogonal polarization modes (Rankin, Campbell & Backer 1974; Manchester, Taylor & Huguenin 1975; hereafter OPMs), many assumed that the 'primary' polarization mode must be parallel. This easy presumption was dashed in the new millennium by X-ray imaging of the Vela pulsar (Helfand, Gotthelf & Halpern 2001; Radhakrishnan & Deshpande 2001) where arcs indicated the orientation of the source's rotation axis Ω relative to its polarization and PM directions. Surprisingly, the radiation was polarized orthogonally to the magnetic field *B* plane, a circumstance confirmed for the radio emission by Johnston I.

For most pulsars, the direction of the rotation axis Ω on the sky must be deduced from the electric vector orientation of its radiation at a rotational phase thought to represent the magnetic axis longitude. At this 'fiducial' instant, a pulsar's beam faces the Earth squarely and the projected magnetic field associated with its emission is parallel to Ω. Thus, the 'fiducial' polarization position angle (hereafter PPA) PA_0 is measured and referred to infinite frequency as a proxy for the (unseen) orientation of the rotation axis Ω. Values

★ E-mail: joanna.rankin@uvm.edu

Table 1. Proper motions, rotation measures and absolute polarization angles for the 33 pulsars and calibrators.

PSR Bname	PSR Jname	Period P (s)	Age $\log(\tau)$ (yr)	Proper motion PA_v (deg)	Ref.	Rotation measure Previous (rad m^{-2})	Ref.	measured (rad m^{-2})	Fiducial PA_0 (deg)	Fig.	Ψ (deg)
B0011+47	J0014+4746	1.241	7.54	+136(3)	1	–	–	−8.7(11)	+43(7)	1	−87(8)
B0136+57	J0139+5814	0.272	5.61	−131(1)	2	−90(4)	1	−93.2(4)	+43(3)	1	+6(3)
B0149−16	J0152−1637	0.833	7.01	+173(2)	1	+2(1)	2	+6.6(50)	−86(9)	1	+80(15)
B0320+39	J0323+3944	3.032	7.88	+158(8)	3	+58(3)	1	+56.3(10)	−34(2)	2	+12(9)
B0458+46	J0502+4654	0.639	6.26	−45(19)	3	−48(6)	1	−175.2(10)	−9(2)	2	–36(20)
B0906−17	J0908−1739	0.402	6.98	+167(2)	3	−36(6)	3	−32.1(7)	−27(14)	2	+14(14)
B1039−19	J1041−1942	1.386	7.37	−4(12)	1	−16(5)	1	−22.8(5	−12(1)	2	+8(12)
B1112+50	J1115+5030	1.656	7.02	+157(2)	3	+3.2(5)	4	−0.1(8)	−35(2)	2	+11(3)
B1237+25	J1239+2453	1.382	7.36	−65(1)	4	–0.3(1)	5	+3.9(3)	−20(1)	A1	
B1322+83	J1321+8323	0.670	7.27	−76(14)	3	–	–	−23.2(11)	+26(3)	2	+78(15)
B1325−43	J1328−6038	0.533	6.45	+3(5)	1	−41(3)	6	−22.9(9)	−4(7)	3	+7(9)
B1508+55	J1509+5531	0.740	6.37	−130(1)	2	+0.8(7)	7	+3.1(4)	+3(2)	A1	
B1540−06	J1543−0620	0.709	7.11	–103(10)	1	+4(4)	1	−1.8(8)	+66(2)	3	+10(10)
B1703−40	J1707−4053	0.581	6.68	+5(35)	5	−207(25)	8	−179.7(5)	+5(1)	3	0(35)
B1718−02	J1720−0212	0.478	7.96	−178(9)	1	+17(3)	1	+6.0(15)	−8(4)	3	+10(9)
B1718−32	J1722−3207	0.477	7.07	−179(7)	5	+90(7)	1	+70.4(5)	−62(1)	3	+63(7)
B1732−07	J1735−0724	0.419	6.74	−5(3)	1	+8(3)	1	+34.5(3)	−22(1)	3	+17(4)
B1757−24	J1801−2451	0.125	4.19	+270(10)	6	+637(12)	9	+605.7(5)	−65(2)	4	–25(10)
B1800−21	J1803−2137	0.134	4.20	+3(5)	5	−27(3)	10	−36.1(2)	+15(1)	4	−12(5)
B1821−19	J1824+1945	0.189	5.76	–173(17)	5	−303(15)	1	−302.2(7)	+53(2)	4	–46(17)
B1826−17	J1829−1751	0.307	5.94	+172(9)	5	+306(6)	6	+304.7(4)	+11(1)	4	−19(9)
B1839+56	J1840+5640	1.653	7.24	−125(5)	3	−3(3)	1	−5.0(7)	+56(2)	4	−1(5)
B1905+39	J1907+4002	1.236	7.56	+45(10)	3	+7(3)	1	+5.2(3)	+66(1)	4	–21(10)
B1911−04	J1913−0440	0.826	6.51	+166(6)	3	+12(3)	3	+4.6(4)	−20(1)	A1	
B1929+10	J1932+1059	0.227	6.46	+65(1)	7	−6.87(2)	3	−5.8(2)	+78(1)	A1	
B2106+44	J2108+4441	0.415	7.88	+68(26)	1	−146(9)	1	−433.0(6)	+66(7)	5	+2(27)
B2111+46	J2113+4644	1.015	7.35	+113(44)	8	−224(2)	7	−218.7(1)	−86(1)	5	+19(44)
B2148+63	J2149+6329	0.380	7.55	+54(12)	3	−160(7)	1	−156.5(3)	−58(20)	5	–67(23)
B2154+40	J2157+4017	1.525	6.85	+76(1)	2	−44(2)	4	−32.6(30)	+83(7)	5	−7(7)
B2217+47	J2219+4754	0.538	6.49	–158(10)	9	−35.3(18)	7	–	+65(4)	5	–44(11)
B2224+65	J2225+6535	0.683	6.05	+52(1)	3	−21(3)	1	−14.7(7)	−43(5)	5	−85(5)
B2255+58	J2257+5909	0.368	6.00	+106(12)	5	−322(11)	1	−323.5(4)	+24(3)	6	+82(12)
B2310+42	J2313+4253	0.349	7.69	+76(1)	2	+7(2)	1	+4.4(1)	+18(10)	6	+58(10)
B2319+60	J2321+6024	2.256	6.71	–	–	−230(10)	1	−232.6(2)	−60(1)	6	–
B2324+60	J2326+6113	0.234	7.02	+63(24)	8	−221(10)	1	−220.7(3)	+49(1)	6	+14(24)
B2327−20	J2330−2005	1.644	6.75	+86(2)	1	+16(3)	1	+9.2(8)	+28(2)	6	+59(3)
B2351+61	J2354+6115	0.945	5.96	+75(9)	3	−77(6)	1	−75.9(4)	+48(1)	6	+27(9)

Proper motion refs: (1) Brisken et al. (2003); (2) Chatterjee et al. (2009); (3) Harrison, Lyne & Anderson (1993); (4) Brisken et al. (2002); (5) Zou et al. (2005); (6) Thorsett, Brisken & Goss (2002); (7) Chatterjee et al. (2004); (8) Hobbs et al. (2004); (9) Lyne, Anderson & Salter (1982).

Rotation measure refs: (1) Hamilton & Lyne (1987); (2) Qiao et al. (1995); (3) Johnston et al. (2005); (4) Manchester (1974); (5) Taylor, Manchester & Lyne (1993); (6) Han, Manchester & Qiao (1999); (7) Manchester (1972); (8) Noutsos et al. (2008); (9) Han et al. (2006); (10) Rand & Lyne (1994).

for PA_0 can be compared with well determined PM directions PA_v, defining the orientation angle $\Psi = PA_v - PA_0$. These studies are necessarily limited, because PM provide only two of the components of a pulsar's velocity. Therefore, for some pulsars that lie in particular directions relative to the Earth and the Galactic plane, lack of this third velocity component results in an incomplete and distorted picture of a pulsar's Ω orientation relative to its PA_v direction. In their 2012 work, Noutsos et al. (2012) modelled the third component of the velocity, and concluded that aligned rather than orthogonal vector orientations were more likely.

In the following sections, we present absolute, infinite-frequency polarization profiles for the 33 sources under study. For 23 of these, the results are new, while 10 other pulsars appear below in order to confirm some aspect of the earlier analyses. The pulsars were studied and classified in terms of the system described in Rankin (1993a,b) in order to better understand the emission geometry and the relationship of the polarization traverses to the fiducial longitude. Wherever possible, the PPA traverse was fitted using the rotating-vector model (Radhakrishnan & Cooke 1969; hereafter RVM) and referred to infinite frequency using an RM stemming from our observation (or in several cases published values). Section 2 outlines our observational procedures, and in Section 3 we discuss the profile analyses conducted to determine the fiducial longitudes. Section 4 presents the fiducial PPA analyses, and Section 5 a summary and discussion of the results.

2 OBSERVATIONS

The observations were carried out in the summer of 2011 using the 100-m Robert C. Byrd GBT and the Green Bank Ultimate Pulsar Processing Instrument (GUPPI) in coherent filterbank mode. The dates, resolutions and lengths of the various observations are given

in Table A1. Full-Stokes spectra were acquired in an 800 MHz bandwidth centred at 1500 MHz radio frequency; the ∼1200–1300 MHz airport radar analogue filter was used, resulting in a ∼700 MHz effective bandwidth. The filterbank frequency resolution was 1.5 MHz, or 512 channels across the full band. The data were coherently dedispersed in real time using the catalogued[1] dispersion measure for each pulsar to remove in-channel dispersive smearing, then integrated in time for 20 μs per spectrum and recorded to disc. The filterbank data were 'folded' modulo the current apparent pulse period into the final full-Stokes pulse profiles. In all cases the final profile resolution was 1/2048 of the pulsar's rotation period (hereafter P) and these resolutions are also given in Table 1. The filterbank files were inspected for radio-frequency interference (hereafter RFI) and the corrupted areas masked out in frequency and time.

Flux and polarization calibration were performed using the PSRCHIVE software package (Hotan, van Straten & Manchester 2004). Paired with each pulsar, an observation of a locally generated standard noise source was recorded to determine the flux density scale. The equivalent noise-source flux density was determined during our project via observation of the unpolarized quasar J1445+0958, with an assumed flux at 1500 MHz of 2.32 Jy (Condon et al. 1998). From a 3-h observation of the pulsar B0450+55, taken as part of a different observing programme using an identical instrumental setup, the parallactic angle rotation with respect to the telescope was used to solve for the receiver system's intrinsic polarization cross-coupling matrix, following van Straten (2004). From the calibrated profiles versus frequency, rotation measures (RM) were determined using the PSRCHIVE program 'RMFIT': an initial RM was determined by finding the RM value that maximized the total linearly polarized flux in the frequency-averaged profile. After applying the initial RM, the full band was averaged into upper and lower halves, and the weighted mean position-angle difference between the two halves was used to find the final RM and its uncertainty (e.g. Han et al. 2006). RM determinations for all sources are tabulated in Table 1. The calibrated profiles were then RM de-rotated, corrected for parallactic angle, and integrated over the full band – providing the basis for the analyses described in the following sections.

3 POLARIZATION PROFILE ANALYSIS

Absolute fiducial PPA determinations require accurate measurements of three different types: (a) absolute polarimetry (PPAs measured counterclockwise from north on the sky) at the frequency of observation; (b) RM values to refer the PPAs to infinite frequency and (c) profile analyses to estimate the 'fiducial' longitude of a pulsar's magnetic axis so that the 'fiducial' PPA can then be computed.

Many details of our three-fold analyses are presented in the appendix. The results of the observational calibrations and reductions from the GBT are given in Figs 1–6 and Fig. A1 below. Each figure gives results for up to six pulsars. The total power, linear and circular polarization of the profile are given in the lower panels of each display, while the PPA information is given in the upper panels. Here the PPAs have been referred to infinite frequency, and a horizontal line showing the PM direction PA_v is also indicated (red, or blue if shifted by 180°).

Two different approaches were used to estimate the fiducial longitude and thus the fiducial PPA PA_0, and in most cases they gave

[1] ATNF pulsar catalogue (Manchester et al. 2005); http://www.atnf.csiro.au/research/pulsar/psrcat

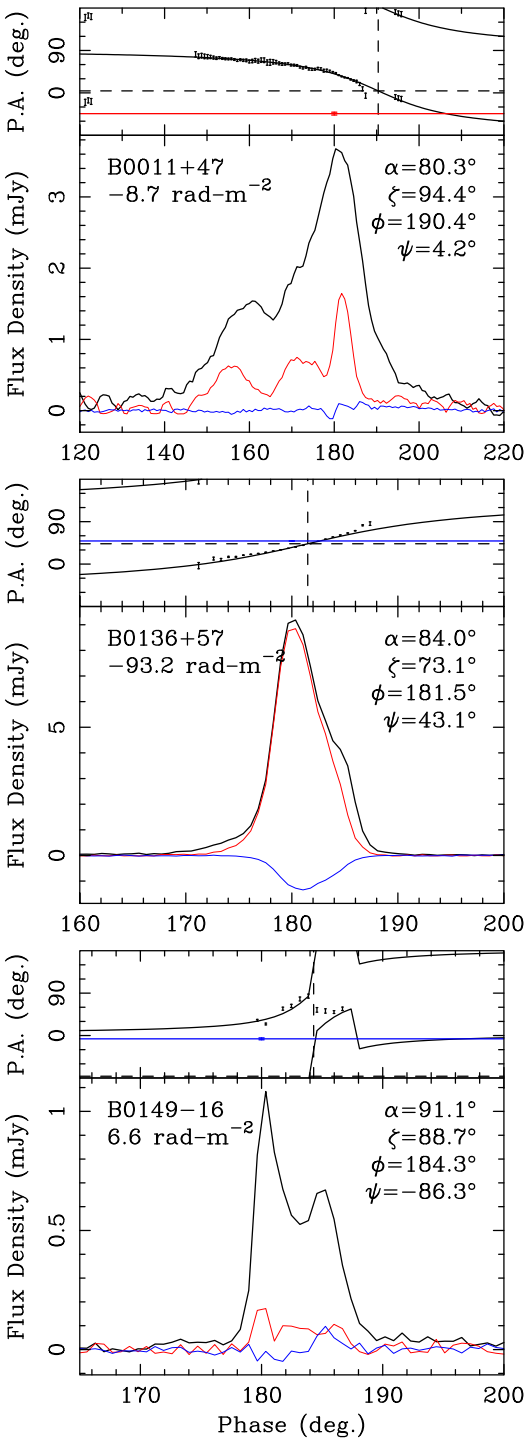

Figure 1. Polarization profiles for pulsars B0011+47, B0136+57 and B0149−16. The lower panels give the total power (Stokes I; heavy black curve), total linear polarization (Stokes L; red curve) and total circular polarization (Stokes V; blue curve). The upper panels give the measured polarization position-angle (hereafter PPA) values – derotated to infinite frequency according to the specified RM – with their errors as well as a fitted curve computed using the RVM. The linear polarization signal-to-noise ratio cutoff for inclusion was 4. The pulsar proper-motion direction on the sky is indicated by a red horizontal line (blue when shifted by 180°.) The pulsar names are given at the upper left and the fitted parameter values at the upper right of the lower panels: magnetic latitude α, sightline circle radius ζ (per the Everett & Weisberg 2001 convention), central longitude ϕ, and fiducial PPA ψ.

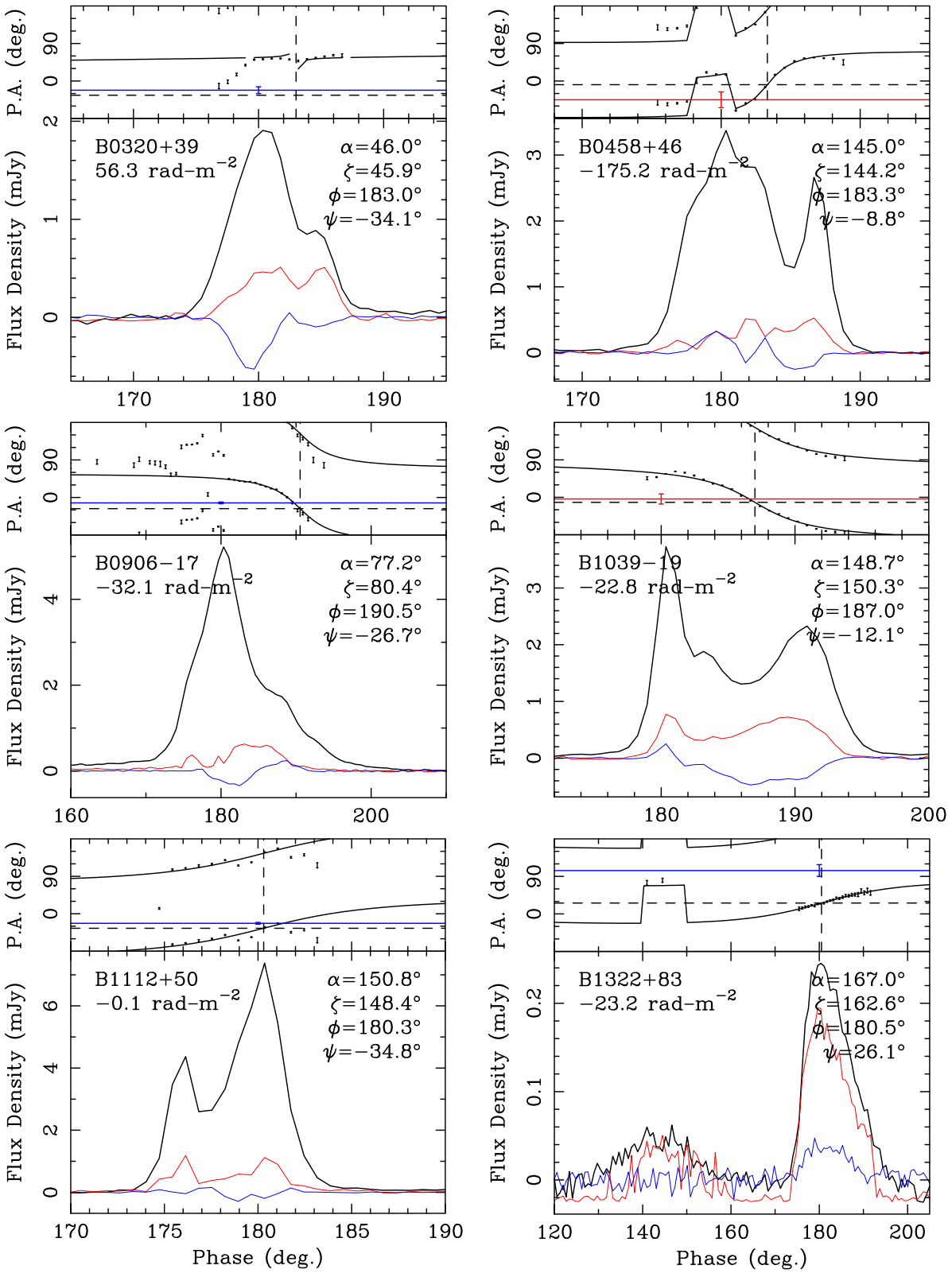

Figure 2. Polarization profiles for B0320+39, B0458+46, B0906−17, B1039−19, B1112+50 and B1322+83 as in Fig. 1.

compatible guidance. First, we reassessed the totality of the available published polarized profile information on the 33 pulsars in an effort to determine the nature of their sightline traverses using the core/double cone model of Rankin (1993a,b) and the other papers of this series. The results of these efforts are discussed in paragraphs on each source in the appendix and summarized in Table A2.

Secondly, we fitted RVM curves to the PPA traverses of each pulsar. These values are given on each plot: the central longitude ϕ

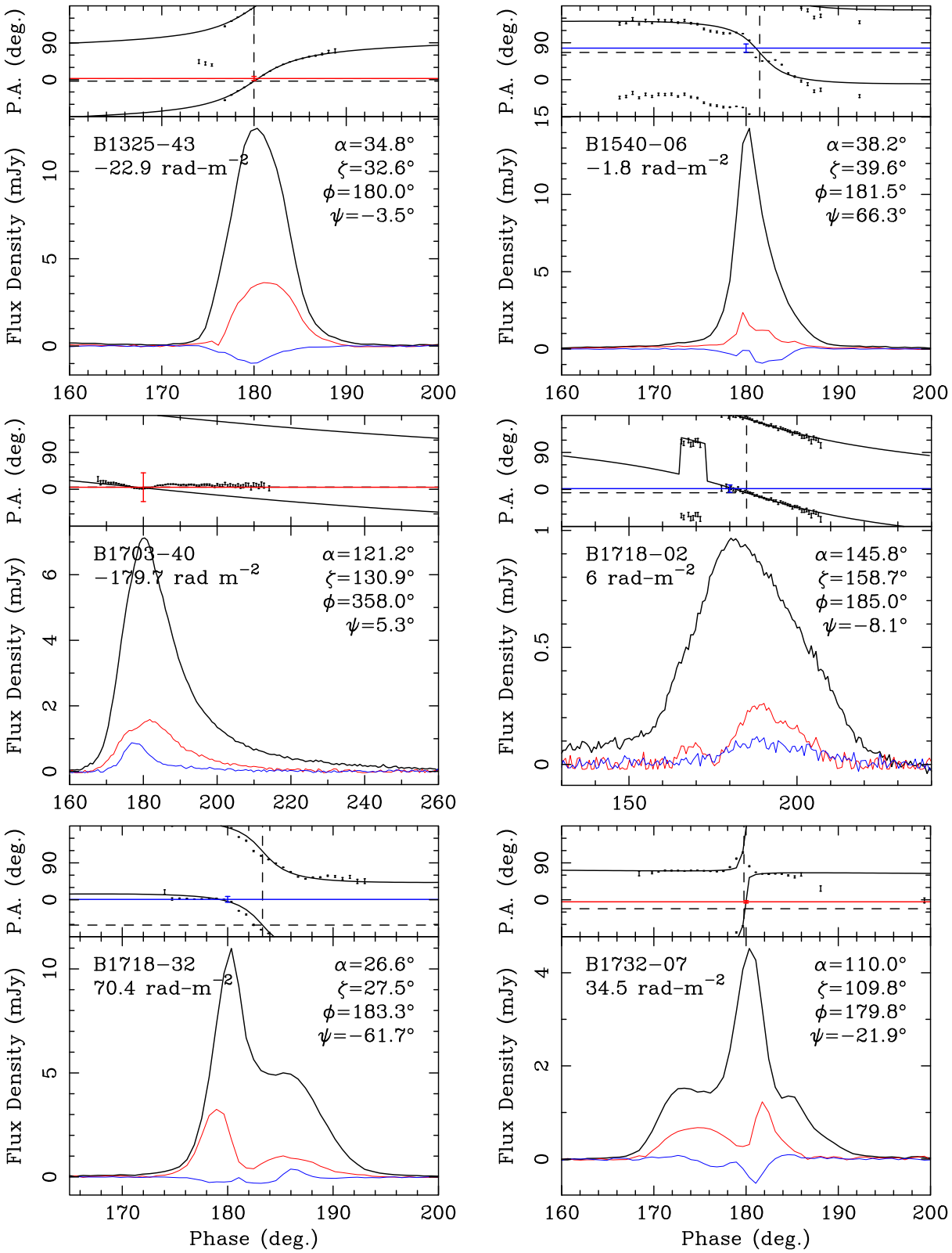

Figure 3. Polarization profiles for pulsars B1325−43, B1540−06, B1703−40, B1718−02, B1718−32 and B1732−07 as in Fig. 1.

and PPA at the central longitude ψ as well as the magnetic latitude α and the sightline circle radius ζ [$=\alpha+\beta$]. The latter two values were always highly correlated with large errors, so only the PPA sweeprate $R = \sin\alpha/\sin\beta$, where β corresponds to the sightline impact parameter, was usefully determined. In most cases the fits were taken as the best estimates of the fiducial longitudes and angles PA_0 that appear in Table 1, though, for some third of the pulsars, the longitude origin was fixed for an analytical consideration, explained

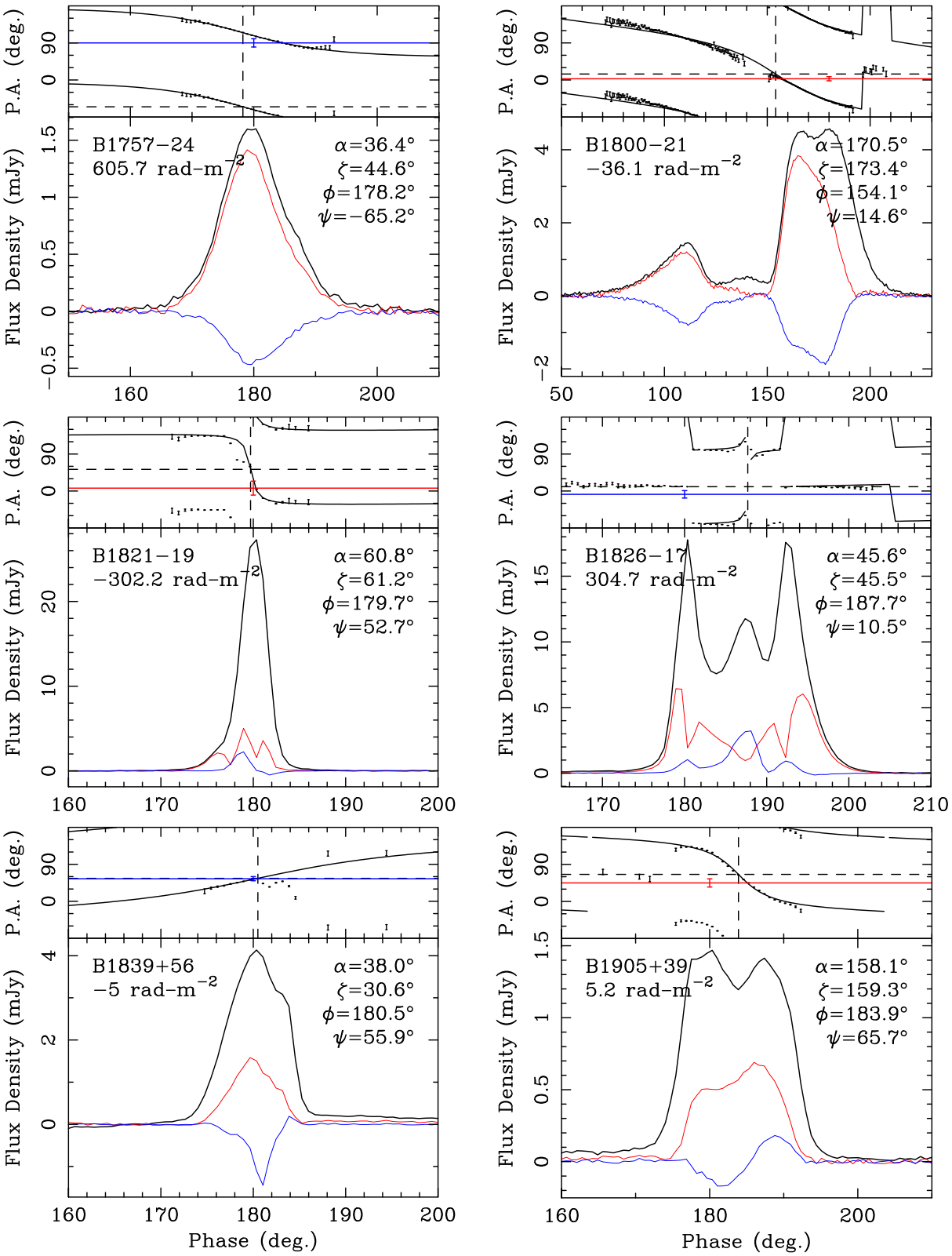

Figure 4. Polarization profiles for pulsars B1757−24, B1800−21, B1821−19, B1826−17, B1839+56 and B1905+39 as in Fig. 1.

when relevant in the appendix. The PA_0 errors reflect both the fitting errors and the RM uncertainties in derotating to infinite frequency. A dashed vertical line on each plot shows the fitted or fixed fiducial longitude. In some cases it was necessary to correct for orthogonal polarization mode 'jumps'; these are indicated as relevant. Low level polarized RFI was at times found to persist in the observations and seemed to affect our RM measurements and/or RVM fits. In such cases the longitude range used for these analyses was restricted to

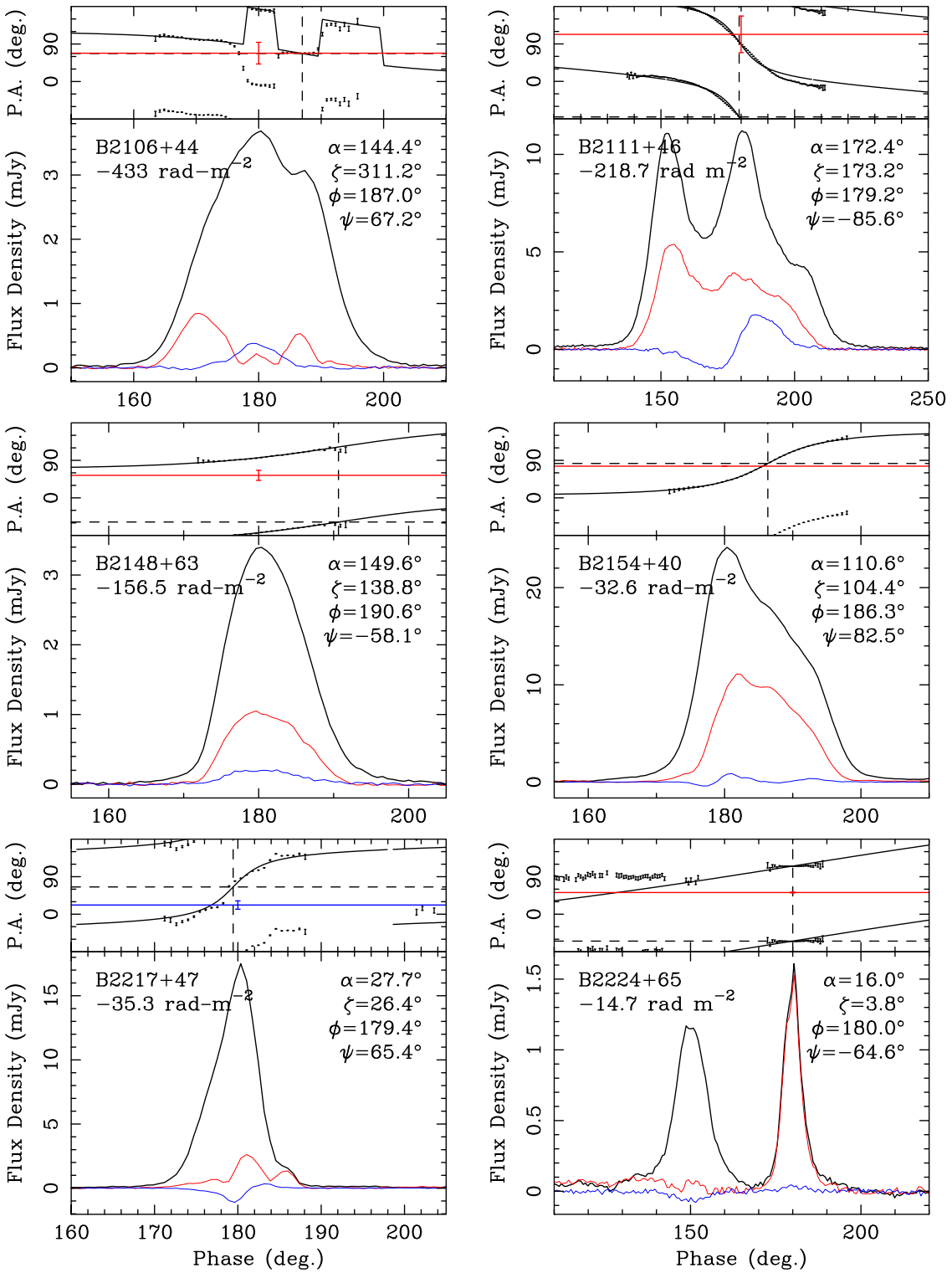

Figure 5. Polarization profiles for pulsars B2106+44, B2111+46, B2148+63, B2154+40, B2217+47 and B2224+65 as in Fig. 1.

avoid possible distortion. These issues are discussed for each pulsar in the appendix.

4 PM & FIDUCIAL PPA ANALYSIS

Four pulsars with well measured absolute polarization angles were included in the observations as calibrators, and several other such sources were included in order to better understand their fiducial geometry. Panels showing the absolute polarization and PM orientations for pulsars B1237+25, B1508+55, B1911−04 and B1929+10 are given as Fig. A1. Not surprisingly, the closest correspondence is for B1929+10, where the +78° PA_0 fit (to the primary PPA mode) agrees with Johnston I's value of −11(1)° (relating to the secondary) within a joint error of 1°. B1508+55's PA_0 value

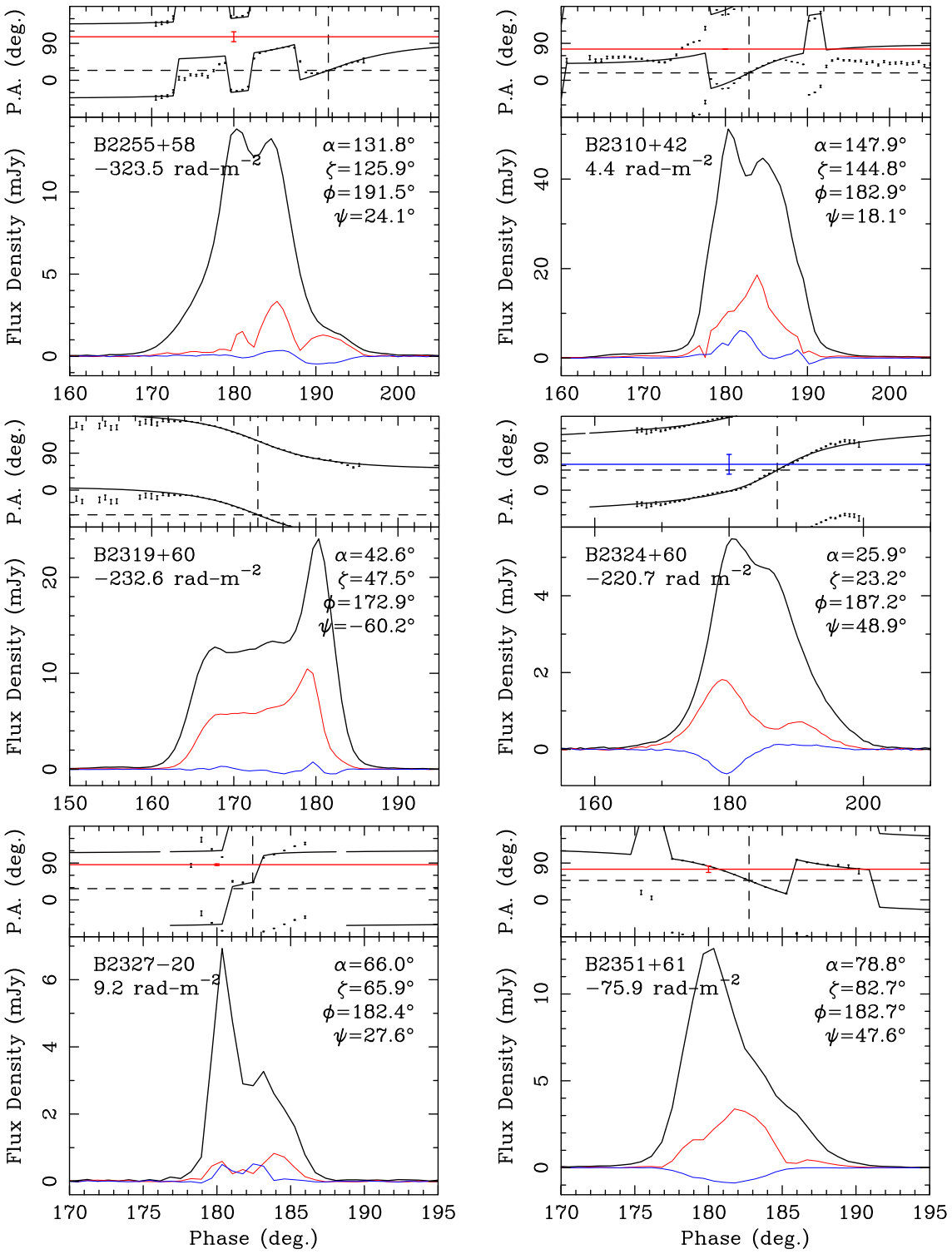

Figure 6. Polarization profiles for pulsars B2255+58, B2310+42, B2319+60, B2324+60, B2327−20 and B2351+61 as in Fig. 1.

agrees with that of Morris et al. (1979) within 2° with an uncertainty of 7°, and the PA_0 for B1911−04 is identical to that of Johnston I (at a longitude of −3°) within ±8°. Only for B1237+25 does the fiducial PA_0 disagree with the above by 8°±1°; this goes to zero if the apparently too large RM value used here is in error.

5 SUMMARY AND DISCUSSION

A three part analysis was undertaken to compare the linear polarization of 33 observed pulsars with published PM for these sources. The relationship between the PM direction PA_v and the fiducial polarization angle direction PA_0 is given in Table 1 for the 33 pulsars under study. These values reflect the analyses discussed above as

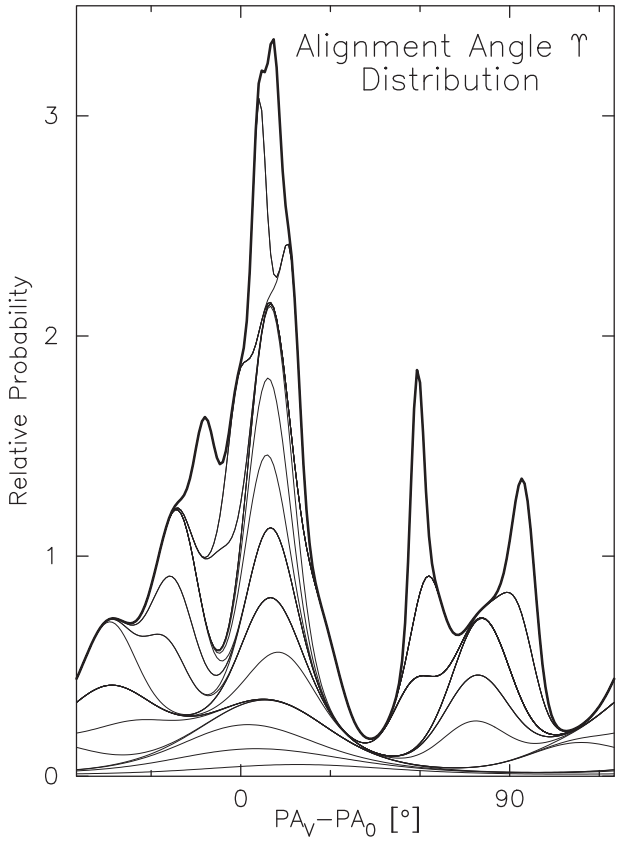

Figure 7. Distribution of alignment angles Ψ [=PA$_v$−PA$_0$] for the 33 pulsars in Figs 1–6. Here, the alignment of each pulsar is represented by a 180°-von Mises function with peak Ψ and standard deviation corresponding to its error value. Each function has equal area such that the total area of the cumulative distribution (dark curve) is normalized to the area of the region below unity. These 33 pulsars show a broad distribution with some clustering near 10° and 80°.

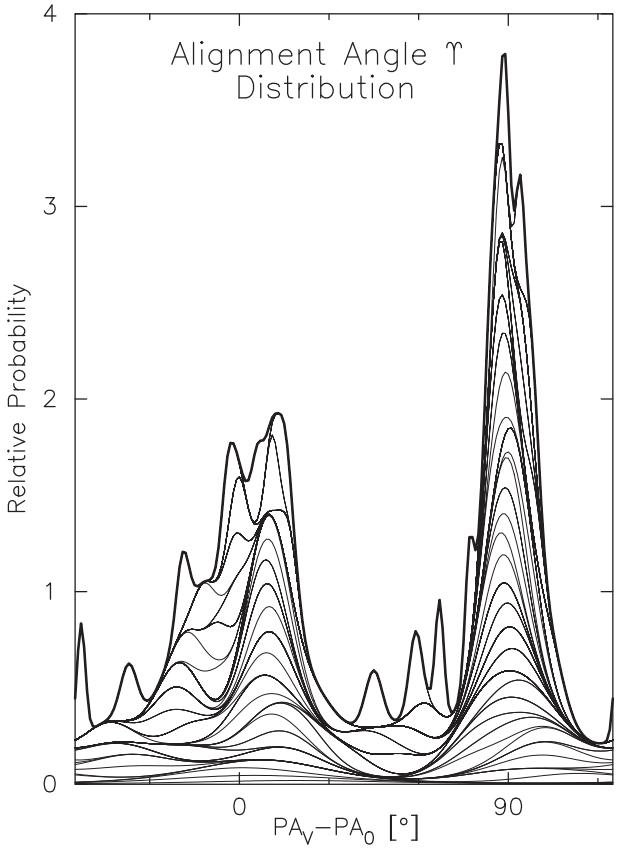

Figure 8. Distribution of alignment angles Ψ as in Fig. 7 for the entire population of 87 pulsars for which this has been computed in Johnston I/II, Rankin (2007), Noutsos et al. (2012) and this paper. Here, the aggregate curve exhibits peaks around 0° and 90° as well as a broad distribution of other well determined values.

well as the specific circumstances of each pulsar as discussed in the appendix.

Ten of the sources had been observed previously and were included here either to check or extend the interpretation: B0906−17 (Johnston I), B1732−07, B1757−24 and B2327−20 (Johnston II), with the remainder from Rankin (2007) quoting either Xilouris et al. (1991) or Morris et al. (1979). For B0906−17 the fiducial longitude was estimated; for the second group Johnston II's values were confirmed or reinterpreted. For pulsars B2154+40 and B2217+47, we reconfirm Morris et al.'s values within the joint errors. For the remaining Xilouris et al. pulsars, two are confirmed with smaller errors and two are reinterpreted.

Supporting previous conclusions, the polarimetry results from this enlarged sample are comparable overall to the populations studied in Johnston I and II, with Johnston I representing a somewhat younger population than Johnston II. As shown in Fig. 7, the alignment values fall into three groups. About half of the sources show alignments such that their fiducial polarization directions are parallel to their PM directions within a few degrees. Some others appear to have orthogonal alignments, and the remaining third show intermediate alignments, some of them seemingly well determined and accurate. The values in the figure are represented by 180°-von Mises functions centred on the alignment value Ψ [=PA$_v$−PA$_0$] with widths reflecting their respective errors. The values are plotted bottom to top in order of decreasing error, so several pulsars with small errors produce prominent 'spikes'. The apparent misalignment of these sources is likely strongly affected by the missing radial component of the velocity; in the case of B1237+25 proximity to the North Galactic Pole may have an effect. The lack of alignment in pulsar B1508+55 is largely explained by the work of Chatterjee et al. (2005).

Fig. 7, along with the results of the earlier papers, appears to argue strongly that many pulsars do exhibit velocity vectors aligning closely with their magnetic axes. However, inherent ambiguities remain due both to the lack of knowledge about the active orthogonal emission mode as well as the missing radial component of the pulsar's velocity. Comparison of alignment values for 54 pulsars with three-component simulations by Noutsos et al. (2012) found a strong case for pulsar spin-velocity alignment.

Along with Johnston I, II, and Rankin (2007), Noutsos et al. (2012) and this effort brings the number of pulsars with well-studied fiducial polarization alignments to 87. Absolute polarimetry measurements have now been carried out for most of roughly 100 normal (not millisecond) pulsars which currently have accurately determined PMs. Fig. 8 shows the overall alignments of this larger group of pulsars. Note that the alignments again fall into peaks near 0° and 90°, but here the peaks are sharper, in part perhaps reflecting the properties of the somewhat younger pulsars first studied in Johnston I.

That the population of alignments shows roughly equal groups at near 0°and 90° is reflective of orthogonal mode emission in

pulsars, and our inability to distinguish between the two modes has frustrated further analysis and interpretation. However, apparently the two modes can be effectively distinguished in core emission components. In a recent study Rankin (2015) has shown that core emission is polarized perpendicular to the projected local magnetic field direction, thus representing the extraordinary (X) propagation mode. This study draws on a population of nearly 50 pulsars with core components, including 11 of those above. Pulsars with strong core emission represent the youngest profile class. X-mode core radiation seems to arise at lower altitudes within a pulsar's polar flux tube and then to in part be converted to O-mode core radiation at higher altitudes. That X-mode core emission is the lowest altitude 'parent' emission in turn implies that it must be tertiary to both the primary particle acceleration and the formation of any secondary plasma. It also implies that pulsar PMs tend to be parallel to pulsar rotation axes, suggesting that supernova 'kicks' outweigh binary disruption as a mechanism for pulsar velocities. Finally, that the orthogonal modes can be identified in some pulsars as reflecting radiation either orthogonal or parallel (X- or O-mode) to the local field opens the possibility of studying pulsar radiation in more physical and plasma-physical terms.

ACKNOWLEDGEMENTS

The authors wish to thank Dr Aris Noutsos for his advice and assistance with the analyses and Professor Joel Weisberg for providing ionospheric RM estimates. Portions of this work were carried out with support from US National Science Foundation Grant AST 08-07691 and PIRE award 0968296. The GBT is operated by the National Radio Astronomy Observatory under contract to the US National Science Foundation. This work used the NASA ADS system.

NOTE ADDED IN PROOF

The Hobbs et al. (2004) PMs for pulsars B2111+46 and B2324+60 are both given in ecliptic coordinates and have been converted to equatorial coordinates in Table 1 by rotations of -23 and -45°, respectively. The PAv and PAo values for B2111+46 in Table 1 of Rankin (2015) are incorrect, the one due to an incorrect equatorial rotation and the latter because of a dropped sign.

REFERENCES

Basu R., Mitra D., Rankin J. M., 2015, ApJ, 798, 105 (ET X)
Blaskiewicz M., Cordes J. M., Wasserman I., 1991, ApJ, 370, 643
Brisken W. F., Benson J. M., Goss W. M., Thorsett S. E., 2002, ApJ, 571, 906
Brisken W. F., Fruchter A. S., Goss W. M., Herrnstein R. M., Thorsett S. E., 2003, AJ, 126, 3090
Chatterjee S., Cordes J. M., Vlemmings W. H. T., Arzoumanian Z., Goss W. M., Lazio T. J. W., 2004, ApJ, 604, 339
Chatterjee S. et al., 2005, ApJ, 630, L61
Chatterjee S., Brisken W. F., Vlemmings W. H. T., Goss W. M., Lazio T. J. W., Cordes J. M., Thorsett S. E., 2009, ApJ, 698, 250
Condon J. J., Cotton W. D., Greisen E. W., Yin Q. F., Perley R. A., Taylor G. B., Broderick J. J., 1998, AJ, 115, 1693
Deshpande A. A., Ramachandran R., Radhakrishnan V., 1999, A&A, 351, 195
Everett J. E., Weisberg J. M., 2001, ApJ, 553, 341
Gould D. M., Lyne A. G., 1998, MNRAS, 301, 253 (GL)
Hamilton P. A., Lyne A. G., 1987, MNRAS, 224, 1073
Han J. L., Manchester R. N., Qiao G. J., 1999, MNRAS, 306, 371
Han J. L., Manchester R. N., Lyne A. G., Qiao G. J., van Straten W., 2006, ApJ, 642, 868
Harrison P. A., Lyne A. G., Anderson B., 1993, MNRAS, 261, 113
Helfand D. J., Gotthelf E. V., Halpern J. P., 2001, ApJ, 556, 380
Hobbs G., Lyne A. G., Kramer M., Martin C. E., Jordan C., 2004, MNRAS, 353, 1311
Hotan A. W., van Straten W., Manchester R. N., 2004, PASA, 21, 302
Izvekova V. A., Kuzmin A. D., Shitov Yu. P., 1982, SvA, 26, 324
Johnston S., Hobbs G., Vigeland S., Kramer M., Weisberg J. M., Lyne A. G., 2005, MNRAS, 364, 1397 (Johnston I)
Johnston S., Kramer M., Karastergiou A., Hobbs G., Ord S., Wallman J., 2007, MNRAS, 381, 1625 (Johnston II)
Lyne A. G., Manchester R. N., 1988, MNRAS, 234, 477
Lyne A. G., Anderson B., Salter M. J., 1982, MNRAS, 201, 503
Malofeev V. M., Izvekova V. A., Shitov Yu. P., 1986, preprint FIAN USSR (MIS)
Manchester R. N., 1972, ApJ, 172, 43
Manchester R. N., 1974, ApJ, 188, 637
Manchester R. N., Taylor J. H., Huguenin G. R., 1975, ApJ, 196, 83 (OPM)
Manchester R. N., Han J. L., Qiao G. J., 1998, MNRAS, 295, 280 (MHQ)
Manchester R. N., Hobbs G. B., Teoh A., Hobbs M., 2005, AJ, 129, 1993
Mitra D., Li X. H., 2004, A&A, 421, 215
Mitra D., Rankin J. M., 2011, ApJ, 792, 92 (ET IX)
Morris D., Graham D. A., Sieber W., Jones B. B., Seiradakis J. H., Thomasson P., 1979, A&A, 73, 46
Morris D., Graham D. A., Sieber W., Bartel N., Thomasson P., 1981, A&AS, 46, 421 (MGSBT)
Noutsos A., Johnston S., Kramer M., Karastergiou A., 2008, MNRAS, 386, 1881
Noutsos A., Kramer M., Carr P., 2012, MNRAS, 423, 2736
Qiao G. J., Manchester R. N., Lyne A. G., Gould D. M., 1995, MNRAS, 274, 572
Radhakrishnan V., Cooke D. J., 1969, Astrophys. Lett., 3, 225 (RVM)
Radhakrishnan V., Deshpande A. A., 2001, A&A, 379, 551
Rand R. J., Lyne A. G., 1994, MNRAS, 268, 497
Rankin J. M., 1993a, ApJ, 405, 285 (ET VIa)
Rankin J. M., 1993b, ApJS, 85, 145 (ET VIb)
Rankin J. M., 2007, ApJ, 664, 443
Rankin J. M., 2015, ApJ, 804, 112 (ET XI)
Rankin J. M., Campbell D. B., Backer D. C., 1974, ApJ, 188, 609
Smith E. M., Rankin J. M., Mitra D., 2013, MNRAS, 435, 1984
Spruit H., Phinney E. S., 1998, Nature, 393, 139
Srostlik Z., Rankin J. M., 2005, MNRAS, 362, 1121
Suleymanova S. A., Shitov Yu. P., 1994, ApJ, 422, 17
Suleymanova S. A., Volodin Yu. V., Shitov Yu. P., 1988, Astron. Zh., 422, 17
Taylor J. H., Manchester R. N., Lyne A. G., 1993, ApJS, 88, 529
Thorsett S., Brisken W. F., Goss W. M., 2002, ApJ, 573, L111
van Straten W., 2004, ApJS, 152, 129
von Hoensbroech A., 1999, PhD thesis, Univ. of Bonn
von Hoensbroech A., Xilouris K. M., 1997, A&AS, 126, 121 (vHX)
Weltevrede P., Stappers B. W., Edwards R. T., 2006, A&A, 445, 243 (WSE)
Weltevrede P., Edwards R. T., Stappers B. W., 2007, A&A, 469, 607 (WES)
Wright G. A. E., Fowler L. A., 1981, A&A, 101, 356
Wright G. A. E., Sieber W., Wolszczan A., 1986, A&A, 160, 402
Wu X. J., Manchester R. N., Lyne A. G., Qiao G. J., 1993, MNRAS, 261, 630 (WMLQ)
Xilouris K. M., Rankin J. M., Seiradakis J. M., Sieber W., 1991, A&A, 241, 87
Zou W. Z., Hobbs G., Wang N., Manchester R. N., Wu X. J., Wang H. X., 2005, MNRAS, 362, 1189

APPENDIX A: CLASSIFICATION AND GEOMETRY

In order to appropriately interpret the PPA traverses of the various pulsars, we consulted the body of available published polarimetry,

Table A1. Date, resolution and length of the observations.

Pulsar	Start date (MJD)	Resolution (ms)	Length (s)
B0011+47	55729.762	0.606	1832
B0136+57	55729.787	0.133	1217
B0149−16	55752.399	0.407	1506
B0320+39	55729.805	1.480	2437
B0458+46	55729.837	0.312	1825
B0656+14	55729.863	0.188	1832
B0906−17	55729.888	0.196	1785
B1039−19	55751.860	0.677	1670
B1112+50	55729.916	0.809	1832
B1237+25	55751.894	0.675	1211
B1322+83	55729.941	0.327	3058
B1325−43	55751.942	0.260	1732
B1508+55	55729.980	0.361	1739
B1540−06	55751.919	0.346	1645
B1703−40	55752.178	0.284	1800
B1718−02	55751.967	0.233	1217
B1718−32	55752.121	0.233	1825
B1732−07	55751.985	0.205	1632
B1757−24	55752.146	0.061	2440
B1800−21	55752.203	0.065	1227
B1821−19	55752.220	0.092	1258
B1826−17	55752.238	0.150	1518
B1838−04	55752.260	0.091	1500
B1839+56	55753.317	0.807	1832
B1905+39	55753.342	0.604	2034
B1911−04	55752.281	0.403	1525
B1929+10	55752.110	0.111	605
B1929+10	55753.397	0.111	605
B2106+44	55753.408	0.203	1825
B2111+46	55753.433	0.496	1825
B2148+63	55729.631	0.186	2231
B2154+40	55729.661	0.745	1525
B2217+47	55729.682	0.263	1529
B2224+65	55729.703	0.333	2372
B2255+58	55729.733	0.180	959
B2310+42	55729.748	0.170	916
B2319+60	55752.310	1.102	1217
B2324+60	55752.328	0.114	1620
B2327−20	55752.376	0.803	1645
B2351+61	55752.350	0.461	1620

the profile classifications in Rankin 1993a,b (hereafter ET VIa,b) and occasionally the fluctuation spectra of Weltevrede, Stappers & Edwards 2006 (hereafter WSE) and Weltevrede, Edwards & Stappers 2007 (hereafter WES).

B0011+47: little is known about this source. Our profile in Fig. 1 together with those of Gould & Lyne (1998, hereafter GL) suggest a triple ***T*** profile with a weak trailing 'outrider', and the WES/WSE fluctuation spectra provide weak support for this interpretation. R, the ratio of sin α to sin β, is -5.7 deg deg^{-1} both in Table A2 and near this value in the fitted RVM curve in the above figure. This said, the fit is poor, and the PPA inflection point should not fall as late as it does in such a slow pulsar. We thus take the fiducial longitude as falling near the peak of the profile at 181° where the PPA is +43°.

B0136+57: seems to be reliably classified as having an $\boldsymbol{S}_t$ profile on the basis of weak conal 'outriders' visible in the 1.7–5 GHz band. The nominal geometry in ET VI using the core-width information (see Table A2) then provides a basis for the PPA fitting in Fig. 1. This fitting, however, seems misleading as the inflection point falls far too late to be reliable. We therefore took the fiducial longitude to be near the centre of the central (putative core) component at a longitude of 181°.5, where the PPA is +43°. Noutsos et al. (2012) find a very similar fiducial longitude.

B0149−16: was classified as featuring a triple ***T*** profile in ET VI, but our profile in Fig. 1 together mainly with those of GL suggest an evolution more like that of an inner cone double ***D*** profile – a drift feature is reported by WES/WSE (see Table A2). The small fractional linear polarization makes the PPA difficult to track, however both the large early rotation and the OPM dominance shift later are seen in other published profiles (e.g. GL at 408 MHz). The R value given by Lyne & Manchester (1988) of about 30 deg deg^{-1} is born out by the values in the RVM fit. The fiducial longitude is fixed at 183° – again very similar to Noutsos et al.'s (2012) fiducial longitude.

B0320+39: the evidence is strong and consistent that this 3-s pulsar has a conal single $\boldsymbol{S}_d$ profile as shown in Fig. 2. The low-frequency profiles exhibit pronounced bifurcation, and a strong drift feature is seen by Izvekova, Kuzmin & Shitov (1982) and by WES/WSE. The RVM fit suggests a much steeper PPA traverse than was envisioned in ET VI. The PPA rotation on the leading edge seems unreliable because of the depolarization there. We have thus fitted to the flat part of the traverse and assumed an unresolved 180° rotation at around the linear polarization minimum near the 183° fixed inflection point.

B0458+46: ET VI interpreted this profile as ***T***, and the profile of von Hoensbroech & Xilouris (1997, hereafter vHX; see also von Hoensbroech 1999) at 4.9-GHz appears to seal the case. WES/WSE report a flat fluctuation spectrum. None the less, the very small L/I makes the PPA difficult to fit and interpret reliably in Fig. 2. Apparently the PPA slope is positive, but our fitted R value is very different than that in ET VI.

B0906 − 17: may have a triple ***T*** profile. The Johnston I profile at 21 cm, those of GL, and vHX's 4.9-GHz profile suggest this structure most clearly. WES/WSE again report a flat fluctuation spectrum. None the less the low L/I and prominent OPM dominance shift on the leading edge make the PPA difficult to fit, and indeed Johnston I found no satisfactory fit. Several profiles suggest aberration/retardation, and our fit in Fig. 2 strongly verifies its presence. The RVM fit and Table A2 geometries are comparable in terms of the values for the sightline impact parameter β.

B1039 − 19: exhibits a classic double conal (***M*** or c***Q***) profile along with the nearly 180°, 'S'-shaped PPA traverse – and WES/WSE report clear evidence of modulation. This behaviour is very well exhibited in the work of Mitra & Li (2004) and provides a secure basis for RVM fitting and interpretation in Fig. 2. The values for the angular separation of the magnetic and axes α and the sightline impact parameter β compare closely in Table A2 and the above figure.

B1112+50: ET VI classed this star as having an $\boldsymbol{S}_t$ profile, and indeed its core does seem to fall out of the centre of its profile at 21 cm. and above. WES/WSE, however, detect drifting in the first component and Wright, Sieber & Wolszczan (1986) moding and nulling. Overall, little PPA rotation can be seen across the profile in Fig. 2. The β values compare closely in Table A2 and the above figure. No RVM fit, however, suffices to fix the fiducial longitude, so we have fixed it near the core peak at 180° longitude where the PPA is −35°.

B1237+25: is a classic pulsar with a five-component profile, and its three modes were studied in detail by Srostlik & Rankin (2005) and recently by Smith, Rankin & Mitra (2013), where its highly steep PPA traverse is exhibited in its quiet normal mode.

Table A2. Emission-beam geometry of the sample pulsars as in ET VIb, Table 2. Pulsars are given with their classification, magnetic latitude α, PPA sweeprate $|\Delta\chi/\Delta\phi|_o$ [$=R=\sin\alpha/\sin\beta$], and sightline impact angle β. Outside, half-power conal component widths $\Delta\Phi$, their corresponding radii ρ, and β/ρ are given for the inner and outer cones, respectively, as appropriate using ET VI: equation (4). Finally, characteristic heights are estimated for the two cones using ET VI: equation (6). Bold α values are estimated using the core-component width relation ET VI: equation (1). Measurements are compiled from ET VI, IX, and Basu, Mitra & Rankin (2015, hereafter ET X).

PSR	Class	α (°)	Sweeprate $\lvert\Delta\chi/\Delta\phi\rvert_o$ (deg deg^{-1})	β (°)	Inner $\Delta\Phi$ (°)	Inner ρ (°)	Inner β/ρ	Outer $\Delta\Phi$ (°)	Outer ρ (°)	Outer β/ρ	Inner r (km)	Outer r (km)
B0011+47	T?	10	−5.7	−1.7	45	3.9	−0.44	–	–	–	128	–
B0136+57	St	32	+5.3[a]	+7.5	∼13	8.6	0.87	–	–	–	129	–
B0149−16	D?	84	+30[a]	+1.9	8.2	4.5	0.42	–	–	–	113	–
B0320+39	Sd	69	+23	+2.3	–	–	–	∼5	3.3	0.70	–	221
B0458+46	T?	14	+2.2	+6.4	–	–	–	∼20	7.0	0.91	–	211
B0906−17	arT	31	−6?	4.9	17?	6.8	0.73	–	–	–	124	–
B1039−19	M	31	−18[a]	+1.7	∼13	3.8	0.43	17	4.8	0.34	136	214
B1112+50	St?	**30**	**+10.1**	2.8	7	3.4	0.84	–	–	–	126	–
B1237+25	M	53	−149	−0.3	8.6	3.5	−0.09	12.3	4.9	0.06	110	220
B1322+83m	St?	**14**	**+2.8**	5.1	12?	5.4	0.95	–	–	–	130	–
B1325−43	St?	–	–	–	–	–	–	–	–	–	–	–
B1508+55	T	45	−15	−2.7	11	4.7	−0.58	–	–	–	109	–
B1540−06	Sd	59	−14?	3.5	9?	5.3	0.67	–	–	–	131	–
B1703−40	?	–	–	–	–	–	–	–	–	–	–	–
B1718−02	Sd?	23	−12	−1.9	–	–	–	43	8.2	−0.23	–	214
B1718−32	D?	30	∞	0.0	24?	6.0	0.0	–	–	–	114	–
B1732−07	T?	**54**	∞	0.0	17	6.8	0.0	–	–	–	131	–
B1757−24	St?	–	–	–	–	–	–	–	–	–	–	–
B1800−21	T/M?	16	−1.8	−8.8	88	11.9	0.74	–	–	–	126	–
B1821−19	St?	70	−36	−1.5	–	–	–	–	–	–	–	–
B1826−17	T?	39	+50[a]	+0.7	∼24	7.7	0.09	–	–	–	120	–
B1839+56	T	38	∞	0.0	∼11	3.4	0.0	–	–	–	126	–
B1905+39	M	33	−15[a]	2.1	∼12	4.0	0.53	16.4	5.1	0.41	131	214
B1911−04	St	64	−27[a]	−1.9	9.8	4.8	−0.40	–	–	–	125	–
B2106+44	D?	38	∞	0.0	∼22	6.8	0.0	–	–	–	127	–
B2111+46	T	9	−6.7[a]	1.4	–	–	–	66	5.8	0.24	–	229
B2148+63	Sd	13.6	+1.5[a]	9.0	–	–	–	13.9	9.3	0.97	–	217
B2154+40	cT?	21	+8	+2.6	–	–	–	20.1	4.6	0.56	–	214
B2217+47	St	**42**	+8.5	4.5	12.0	6.1	.73	–	–	–	135	–
B2224+65	St?	**27**	**–3.6**	4.9	–	–	–	–	–	–	–	–
B2255+58	St	24	–	–	–	–	–	–	–	–	–	–
B2310+42	M?	56	+7	+6.8	9.7	8.0	0.85	∼15	9.4	0.73	148	204
B2319+60	cQ?	18	−8[a]	+2.2	∼10	2.8	0.80	19	3.9	0.58	117	225
B2324+60	St?	62	6?	+8.5	∼7	9.0	0.94	–	–	–	127	–
B2327−20	T	**66**	**+43**	1.2	7.0	3.4	0.35	–	–	–	128	–
B2351+61	?	65	−12	−4.3	–	–	–	∼9	5.9	−0.73	–	219

Note. [a]Values from Lyne & Manchester (1988).

The pulsar was also among those whose absolute PPA alignment was determined in Johnston I. It was included here in Fig. 2 as a diagnostic of the polarimetry and PPA fitting.

B1322+83: features a wide 'double' profile which Mitra & Rankin (2011, hereafter ET IX; and Basu et al. 2015, hereafter ET X) interpreted as consisting of a precursor and a trailing single profile (see their fig. A3, lower left). WSE found that the source has a flat fluctuation spectrum; the assumption is that the trailing feature is a $\boldsymbol{S}_t$ profile. Moreover, the PPA traverse is flat under the precursor and linear under the trailing feature, hence we assume that the fiducial longitude coincides with the profile midpoint; see Fig. 2.

B1325 − 43: we find only two published profiles for this pulsar, those of Wu et al. (1993, hereafter WMLQ) and Manchester, Han & Qiao (1998, hereafter MHQ), and these give no clear picture regarding the source's evolution. We rely on the fitted fiducial point from the well-defined PPA traverse in Fig. 3.

B1508+55: absolute PPA measurements were first conducted for this pulsar by Morris et al. (1979, 1981), and it appears to represent an interesting case of misalignment as documented by Chatterjee et al. (2005). We included the pulsar as a diagnostic. Its triple $\boldsymbol{T}$ profile is well studied and modelled in ET VI as a foundation for the fitting in Fig. A1.

B1540 − 06: ET VI classed this pulsar as having a conal single $\boldsymbol{S}_d$ profile, and indeed the strong drift features identified by WES/WSE appears to confirm this. The polarization is slight, but the central PPA traverse agrees with that of GL, possibly indicating an unresolved OPM dominance transition. The linear polarization in the far wings of the profile in Fig. 3 is likely due to RFI.

B1703 − 40: little else is known about this pulsar with a strongly scattered profile even at 21 cm. The PPA traverse is expectedly flat, so we take the fiducial longitude at the profile peak.

B1718 − 02: shows a conal single $\boldsymbol{S}_d$ evolution, an asymmetric single profile near 21 cm. and an unresolved component pair at metre

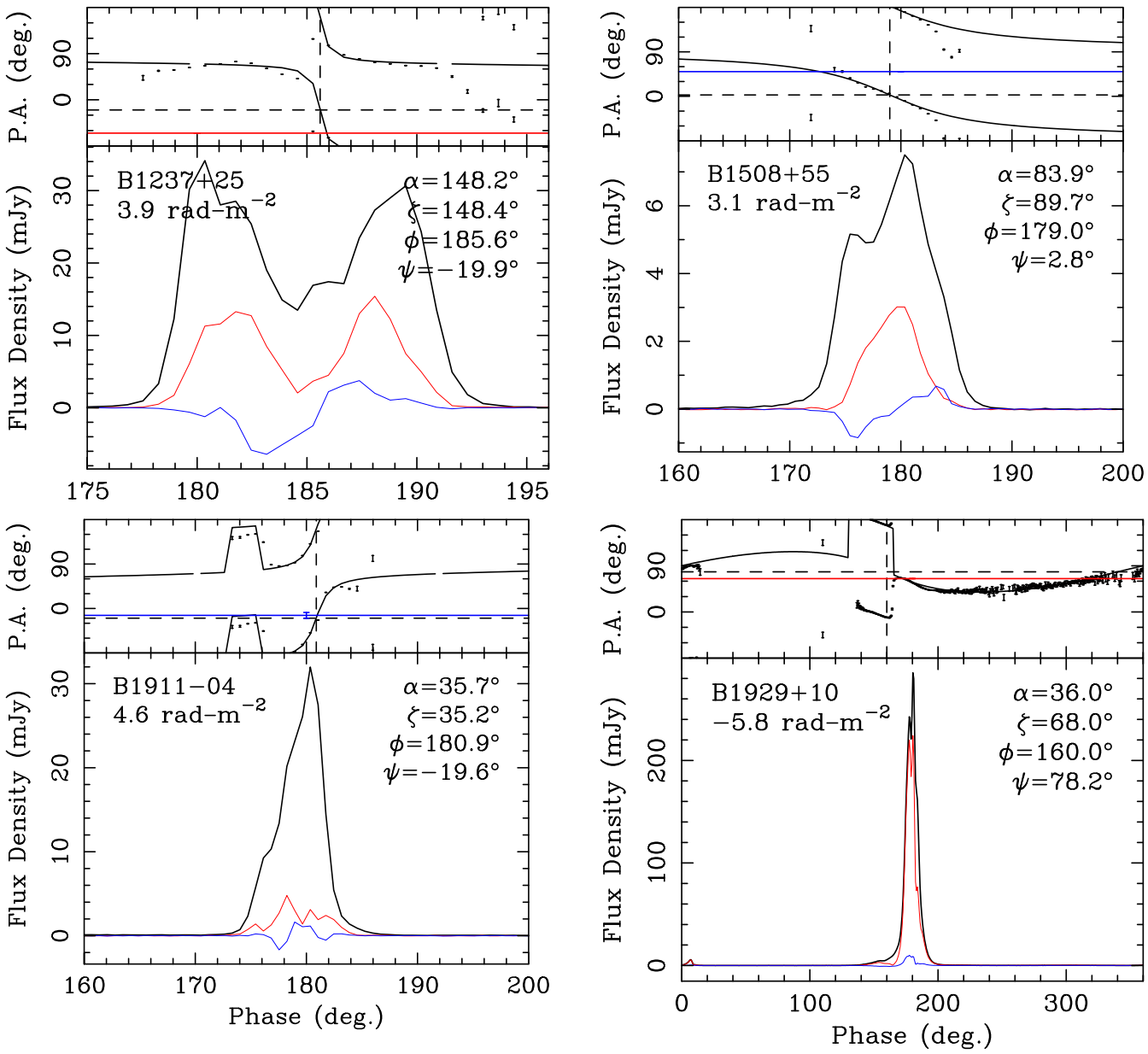

Figure A1. Polarization profiles with absolute PPA information for pulsars B1237+25, B1508+55, B1911−04 and B1929+10 as in Fig. 1, which served as primary calibrators for the absolute polarimetry.

wavelengths; see GL. WSE/WSE noted drift features which appear to confirm the classification. The PPA traverse in Fig. 3, however, is so nearly linear that it poorly fixes the fiducial longitude. A better estimate comes from taking the PPA value at the profile centre near 185° longitude where the fiducial PPA is −8°.

B1718 − 32: little is known about this pulsar; the available profiles (GL, WMLQ) add little to ours in Fig. 3, and there is a lack of fluctuation-spectral information. The PPA traverse is well developed and RVM-like, but the fit is quite poor in terms of χ^2, as is clear from the plot.

B1732 − 07: the evidence seems strong that this pulsar's profile is dominated by a central core component surrounded by one or two pairs of conal 'outriders' – thus it appears to be either of the ***M*** or ***T*** class – though only the inner one is measurable (see Table A2). The best published profiles are those in Johnston II, though GL and vHX are worth inspection. In this context, the PPA traverse strongly resembles that of B1237+25 and thus represents an unresolved steep 180° 'S'-shaped RVM function. The fiducial PPA must then be 90° away from the flat leading and trailing sections in Fig. 3. Noutsos et al. (2012) show a similar profile, but do not accommodate the star's unresolved steep central PPA traverse.

B1757 − 24: little is known about this pulsar, however both GL and Noutsos et al. (2012) confirm a shallow negative-going PPA traverse. The far edge profile break in Fig. 4 and large acceleration potential suggest to the source's classification as $\boldsymbol{S}_t$. The large fractional linear polarization gives a reliable PPA fit.

B1800 − 21: this source's unusual profile has attracted some attention, most notably vHX's comparative study that includes GL's work. This could be classified as an unusual conal double ***D*** profile, but what appears to be a weak core is visible both in our Fig. 4 and GL's 1.41-GHz profile, and the source features a quite large acceleration potential. Thus, a more appropriate classification is ***T***

triple or perhaps ***M***. WES report a flat fluctuation spectrum. The large fractional linear polarization prompts successful fitting for the fiducial longitude.

B1821 − 19: little is known about this pulsar. Most of the GL profiles are poor and show little linear polarization. Their 21 cm profile is their best and largely agrees with our own in Fig. 4. WES/WSE report a flat fluctuation spectrum. The *L* form and large PPA rotation under the pulse suggests a core single $\boldsymbol{S}_t$ profile with weak 'outriders', providing a good foundation for fitting and interpretation of the PPA fiducial centre.

B1826 − 17: this source has a triple profile per ET VI, and the supporting evidence (e.g. GL and MHQ) appears quite strong and consistent. A flat fluctuation spectrum is reported by WES. Interestingly, the PPA traverse in Fig. 4 is completely flat once OPM dominance changes are accounted for – apart from the 180° rotation at the profile centre, similar to that observed for B1237+25.

B1839+56: shows a clear ***T*** triple structure at 102 MHz as per Malofeev et al. (1986, hereafter MIS), however at all higher frequencies these three components appear conflated (GL). Moreover, only at 234 MHz does the PPA traverse seem amenable to RVM fitting; the fit in Fig. 4 has little meaning in that we have fitted only the early linear PPA values and set the fiducial longitude at 180°.5. We assume the fiducial longitude is aligned with the profile peak.

B1905+39: seems to provide a rare example of a conal quadruple c***Q*** profile – that is an ***M*** with little or no core emission. ET VI provides a quantitative model for the source's geometry which gives a secure foundation for the RVM fit in Fig. 4; the fiducial longitude falls very close to the profile centre, as expected.

B1911 − 04: is an excellent example of a pulsar showing a core single $\boldsymbol{S}_t$ evolution – from a symmetrical Gaussian-shaped feature at metre wavelengths (GL) to three-lobed form, with core and conal 'outriders' at high frequency (vHX). The small fractional linear polarization makes the PPA traverse difficult to fit with an RVM curve. After correcting for the OPM offset on the profile's leading edge, the fit in Fig. A1 appears reliable.

B1929+10: is perhaps the best polarization calibrator in the northern sky; we were able to include this source in our programme as a diagnostic on two out of the three days of observation. The polarized profile in Fig. A1 gives an RVM fit that appears reliable under the main pulse (MP), but not so in the region of weak baseline polarization following the MP including the interpulse – the second observation is very similar. For such a strong pulsar, weak RFI would not be discernible in this region but could distort the PPA traverse – this appears to be what has happened here. Other scholars including Blaskiewicz, Cordes & Wasserman (1991) and Everett & Weisberg (2001) found that the MP region had to be unweighted to achieve an acceptable RVM fit – and that the inflection point of such fits fall 20° earlier than the MP peak.

B2106+44: GL's profiles together with our own in Fig. 5 indicate a conal single $\boldsymbol{S}_d$ or perhaps inner cone double ***D*** profile; WES/WSE report a strong low-frequency modulation feature in this source. The pulsar's PPA traverse is very nearly linear, so an RVM fit is difficult and the resulting fiducial longitude not well determined. None the less, the fiducial longitude seems plausible.

B2111+46: this pulsar has a classic core-cone triple ***T*** profile, with the expected steep PPA traverse and substantial fractional linear polarization across its entire profile. The geometric model in ET VI provides a foundation for the fit in Fig. 5, and the fiducial longitude falls near the centre of the profile as expected.

B2148+63: the evidence seems strong per ET VI that this pulsar's profile is of the conal single type $\boldsymbol{S}_d$. It broadens substantially at low frequency (GL, MIS) but scattering may also be a factor. This interpretation is strengthened by the drift modulation detected by WES/WSE. The significant linear polarization (see Fig. 5) defines the PPA traverse well, and the fiducial longitude is decently determined; while it falls late on the trailing side of the profile, some such $\boldsymbol{S}_d$ sources are asymmetric in just this manner.

B2154+40: many published studies indicate that this is a conal profile; either a narrow double ***D*** or conal triple c***T*** as classed by ET VI (see Table A2). Moreover, WES/WSE confirm this interpretation by finding modulation features at both frequencies. The PPA traverse is strong and regular across many octaves [e.g., vHX at 4.9 GHz and Suleymanova, Volodin & Shitov (1988) at 102.5 MHz]; therefore the RVM fit in Fig. 5 appears accurate and identifies a fiducial longitude similar to that of Noutsos et al. (2012).

B2217+47: appears to be a good example of a core-single $\boldsymbol{S}_t$ pulsar (GL), however only at the very highest frequencies do we see any hint of conal 'outriders' (Morris et al. 1981). Some profiles show a PPA traverse rate of about +8.5 deg deg^{-1}, and this provides a basis for the geometric model in ET VI. Apart from the edges, the fit in Fig. 5 appears reliable, and we see only a hint of the variable 'post-cursor' reported by Suleymanova & Shitov (1994); see also ET X.

B2224+65: this source has long been seen as having a conal double profile, however its two components are so dissimilar in form, spectrum and polarization as to render this interpretation unlikely. Again, vHX gives the best comparative discussion, using GL's profiles. All published polarimetry for this source, as well as our own in Fig. 5, show the PPA under the trailing feature to be virtually flat; whereas at high frequency the leading feature is so depolarized that no fit is possible (the early low level linear polarization, including that under the leading feature, is surely corrupted by RFI). In ET IX, the Giant Metrewave Radio Telescope was employed to make a new observation of the pulsar at 325 MHz; the leading MP feature was interpreted as having a core-single $\boldsymbol{S}_t$ profile and the trailing feature interpreted as being a post-cursor. An RVM curve was fitted to both the leading MP and post-cursor (see their fig. A10, upper right; α, $\beta = 166°, -3°.8$). Here, we take the 325 MHz RVM fit as evidence that the fiducial longitude falls very close to the MP peak, and we compute the fiducial PPA in Fig. 5 rotating by the post-cursor PPA +22° as measured at 325 MHz. Our fit is meaningless apart from the −65° reference. ET X casts some doubt on the post-cursor interpretation, but we still believe that magnetic axis longitude falls close to the trailing component.

B2255+58: this source was classified as having a $\boldsymbol{S}_t$ profile in ET VI, and the higher quality three-lobed form in Fig. 6 seems to support this. While the fractional linear polarization is small, the PPA traverse in our profile is similar to what is seen in GL's in this band. Here, we understand the 'wiggles' as OPM dominance switches, resolve them and fit the 'straightened' traverse. The resulting fit in the above figure then seems plausible analytically, though the fiducial longitude falls far after the central putative core component.

B2310+42: is an interesting example of a five-component ***M*** profile according to ET VI. A number of profiles, e.g. Xilouris et al. (1991), suggest triplicity, however weak outer conal features are also seen on the far wings of many profiles; indeed inflections corresponding to the five features can be discerned in our profile in Fig. 6. The PPA traverse is very difficult to interpret, and almost certainly corrupted by low level polarized RFI. GL's 21-cm profile also shows a steep central traverse with OPM dominance shifts on the edges, as well as baseline power far preceding the MP. While this fit is the best that can be achieved with our observation, the inflection point seems unreliable, even if determined with a small formal error.

B2319+60: has a well-studied conal triple c***T*** profile per ET VI, and we see consistent properties over a band of at least four octaves (GL and vHX). Moreover, WES/WSE identify the drift modulation feature and modes that were found in earlier work (Wright & Fowler 1981). The strong linear polarization and steep PPA traverse fix the fiducial longitude near the centre of the profile as expected in Fig. 6.

B2324+60: not much is known about this pulsar beyond the older polarimetry of MGSBT, GL and vHX – in addition to the strong drift feature detected by WES. Interestingly, the better definition of the profile in Fig. 6 suggests that GL's profile was not well resolved. Without other polarimetry of similar quality across the band, it is difficult to make a secure classification. However, such classification seems unnecessary here as the PPA traverse is well defined and the RVM fitting results plausible.

B2327 − 20: has a triple ***T*** profile according to ET VI, based on polarimetry by MGSBT, GL and vHX (see Table A2). The higher quality profiles measured by Johnston II appears to confirm this interpretation. These also show how the large positive roughly 180° PPA swing at metre wavelengths becomes curtailed and distorted at higher frequencies as L/I decreases and profile narrowing conflates the polarization in adjacent regions of the profile. In this context, our profile in Fig. 6 seems to be reasonably measured, however the RVM fit is poor, even after correction for what seems to be the mid-profile OPM dominance shift. None the less, our identification of the pulsar's fiducial longitude is very similar to that of Noutsos et al. (2012).

B2351+61: little study has been given to this pulsar. From the GL and vHX profiles it is clear that it follows a conal single $\boldsymbol{S}_d$ evolution and indeed WES/WSE find evidence of drift modulation. The PPA traverse in Fig. 6 is orderly and regular, apart from the usual OPM dominance shifts on the profile edges. The RVM fit appears reliable as the reduced χ^2 is reasonable.

This paper has been typeset from a TEX/LATEX file prepared by the author.